


Giant Linear Nonreciprocity, Zero Reflection, and Zero Band Gap in Equilibrated Space-Time-Varying Media

Sajjad Taravati

Department of Electrical Engineering, Polytechnique Montréal, Montréal, Québec H3T 1J4, Canada

 (Received 30 December 2017; revised manuscript received 23 March 2018; published 11 June 2018)

This article presents a class of space-time-varying media with giant linear nonreciprocity, zero space-time local reflections, and zero photonic band gap. This is achieved via equilibrium in the electric and magnetic properties of unidirectionally space-time-modulated media. The enhanced nonreciprocity is accompanied by a larger sonic regime interval which provides extra design freedom for achieving strong nonreciprocity by a weak pumping strength. We show that the width of photonic band gaps in general periodic space-time permittivity- and permeability-modulated media is proportional to the absolute difference between the electric and magnetic pumping strengths. We derive a rigorous analytical solution for investigation of wave propagation and scattering from general periodic space-time permittivity- and permeability-modulated media. In contrast with weak photonic transitions, from the excited mode to its two adjacent modes, in conventional space-time permittivity-modulated media, in an equilibrated space-time-varying medium, strong photonic transitions occur from the excited mode to its four adjacent modes. We study the enhanced nonreciprocity and zero band gap in equilibrated space-time-modulated media by analysis of their dispersion diagrams. In contrast to conventional space-time permittivity-modulated media, equilibrated space-time media exhibit different phase and group velocities for forward and backward harmonics. Furthermore, the numerical simulation scheme of general space-time permittivity- and permeability-modulated media is presented, which is based on the finite-difference time-domain technique. Our analytical and numerical results provide insights into general space-time refractive-index-modulated media, paving the way toward optimal isolators, nonreciprocal integrated systems, and subharmonic frequency generators.

DOI: [10.1103/PhysRevApplied.9.064012](https://doi.org/10.1103/PhysRevApplied.9.064012)

I. INTRODUCTION

Reciprocity is a fundamental property of natural materials which governs symmetric wave transmission from a medium. To achieve nonreciprocity, one is required to concurrently break the time-reversal and spatial inversion symmetries. This may be accomplished by artificial structures, including magnetically biased media exhibiting asymmetric permittivity and permeability tensors [1–4], unidirectional transistors [5–7], and nonlinear materials [8–12]. However, magnetically biased nonreciprocal devices suffer from requiring bulky magnets and incompatibility with integrated circuit technology [13], and transistor-based nonreciprocal devices are restricted to low power signals and low frequencies given the limited power handling and operation frequency of the transistors [5,7,14]. Although nonlinear materials provide appropriate nonreciprocity at optical frequencies to high power signals, low-level signals may reciprocally pass through them [15].

Periodic space-time permittivity-modulated media have been recently proposed for nonreciprocal wave transmission and soon acquired a surge of scientific interest thanks to their peculiar way of Lorentz reciprocity

breaking. Such media are endowed with nonreciprocal periodic photonic transitions [16–18] and amplification [19–27]. Unidirectional frequency generation is another interesting property of space-time-modulated media [18,28], where, in contrast to nonlinear harmonic generators, the amplitude of space-time harmonics is not restricted by the classical Manley-Row relations [24]. This property is due to the violation of energy conservation in space-time-modulated media, where external energy is pumped into the system for space-time modulation of the structure [29–31]. The space-time-modulation technique exhibits high isolation and compatibility with circuit technology and integrated optical networks. It has been recently utilized for the realization of microwave and optical isolators [17,18,32–34], nonreciprocal metasurfaces [35–38], nonreciprocal integrated components [30,31], and pure frequency mixing [28].

The contributions of this study are as follows:

- (1) This paper first describes the fundamental limitations of conventional space-time permittivity-modulated media and accordingly introduces the *equilibrated* space-time permittivity- and permeability-modulated medium. The equilibrium is

introduced between the electric and magnetic properties of the medium by identical spatiotemporal modulation of its electric permittivity and magnetic permeability. We show that such an equilibrium results in quite a few unexplored phenomena which may be leveraged for realization of a class of highly efficient microwave and optical integrated components. A rigorous analytical solution is derived for a theoretical description of the scattering and dispersion relation in space-time permittivity- and permeability-modulated media.

- (2) Previously reported space-time-modulated media have focused on the periodic spatiotemporal modulation of the electric permittivity to provide a moderate nonreciprocal frequency generation, mostly in the sonic regime. Here, we show that an equilibrated space-time medium provides highly enhanced nonreciprocity as well as an enhanced sonic regime interval thanks to the stronger space-time transitions to higher-order harmonics. This highly enhanced nonreciprocal frequency generation may be practically achieved at the cost of no more pumped energy into the system, as the space-time permeability modulation may be achieved via the same pumped wave that is modulating the permittivity.
- (3) Conventional, nonequilibrated, space-time-modulated media operate based on spatiotemporal modulation of the electric permittivity, i.e., $\epsilon(z, t) = \epsilon_0 f_{\text{per}}(z, t)$, whereas the magnetic permeability is constant $\mu = \mu_0$. Such media, however, exhibit a space- and time-varying local impedance, i.e., $\eta(z, t) = \eta_0 \sqrt{1/f_{\text{per}}(z, t)}$, resulting in local impedance mismatch in both space and time, which, in turn, yields local reflections in an infinite number of space and time interfaces. This paper shows that an equilibrated space-time-modulated medium exhibits zero space and time local reflections and operates as a reflection-free medium in both the subsonic and sonic regimes.
- (4) In contrast to conventional spatially modulated media, e.g., photonic crystals and Bragg structures, which exhibit horizontal photonic band gaps, conventional periodic space-time permittivity-modulated media introduce asymmetric and oblique photonic band gaps at the space-time synchronization points. The width of these photonic band gaps is proportional to the pumping strength [18,23]. These space-time band gaps may occur at different frequencies and result in significant attenuation (reflection) of the incident wave [18,23,39]. It is shown here that an equilibrated space-time medium exhibits zero-width photonic band gaps. As a result, the incident wave is transmitted through the medium, regardless of its frequency.

- (5) A numerical scheme is provided for deeper investigation of electromagnetic scattering for a general space-time permittivity- and permeability-modulated medium as well as the investigation of the space-time permittivity- and permeability-modulated *sonic regime* slab.

The paper is organized as follows. Section II characterizes the media with periodic space-time-modulated permittivity and permeability. Section III first derives a rigorous analytical solution for the electromagnetic fields inside an unbounded medium with sinusoidally space-time-modulated permittivity and permeability. This section then derives the dispersion relation for such a medium and provides the scattered electromagnetic fields from a slab with sinusoidally space-time-modulated permittivity and permeability. Section III presents the numerical simulation of general space-time permittivity- and permeability-modulated media based on the finite-difference time-domain (FDTD) technique. Section IV exhibits the dispersion diagrams of general space-time-modulated media and investigates the effect of the permeability modulation of zero band gaps. The numerical and analytical results for the scattered fields from a slab with sinusoidally space-time-modulated permittivity and permeability are presented in Sec. V, and then we investigate the effect of equilibrium in the space-time modulations of permittivity and permeability on the nonreciprocity and reflection. Finally, we conclude the paper in Sec. VII.

II. CHARACTERIZATION OF EQUILIBRATED SPACE-TIME-VARYING MEDIUM

Figure 1 depicts a generic representation of the periodic space-time refractive-index-modulated medium with thickness L , periodic unidirectional space-time-modulated electric permittivity

$$\epsilon(z, t) = \epsilon_0 \epsilon_r [1 + \delta_\epsilon \cos(\beta_p z - \omega_p t)], \quad (1a)$$

and periodic unidirectional space-time-modulated magnetic permeability

$$\mu(z, t) = \mu_0 \mu_r [1 + \delta_\mu \cos(\beta_p z - \omega_p t)] \quad (1b)$$

located between two semi-infinite unmodulated media. In Eqs. (1a) and (1b), ϵ_r and μ_r denote the relative electric permittivity of the unmodulated slab, δ_ϵ and δ_μ , respectively, represent the permittivity and permeability pumping strengths, and ω_p and β_p are, respectively, the pump wave temporal and spatial frequencies. The problem with the incident wave propagating toward the $+z$ direction shown at the top of Fig. 1 is called the forward problem “F,” whereas the problem with the incident wave propagating toward the $-z$ direction shown at the bottom of Fig. 1 is called the backward problem “B.” The modulation phase velocity, i.e., $v_p = \omega_p/\beta_p$, may be smaller or greater than the phase velocity of the background medium

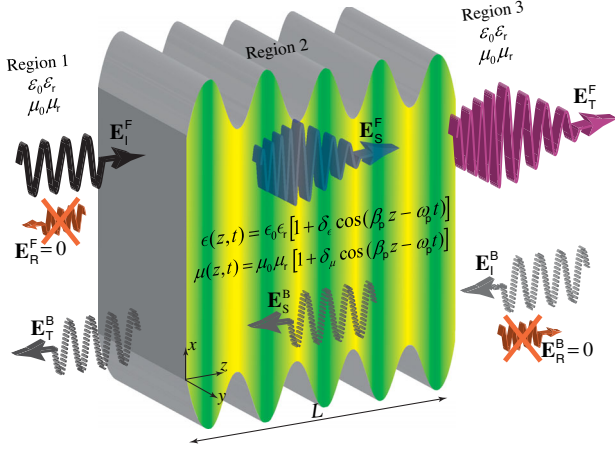


FIG. 1. Schematic representation for electromagnetic scattering from the space-time permittivity- and permeability-modulated slab. Because of the unidirectional modulation of both the electric permittivity and magnetic permeability, the system is nonreciprocal. Considering identical space-time modulation of electric permittivity and magnetic permeability, i.e., $\delta_\mu = \delta_\epsilon$, the slab is in space-time equilibrium, where $\eta = \sqrt{\mu(z,t)/\epsilon(z,t)} = \eta_0\eta_r = \text{const}$. Therefore, the forward and backward incident waves propagate through the slab with zero space-time reflections.

$v_r = c/\sqrt{\epsilon_r\mu_r}$ with $c = 1/\sqrt{\mu_0\epsilon_0}$ being the speed of light in vacuum. The ratio between the modulation and background phase velocities, i.e., $\gamma = v_p/v_r$, represents the space-time velocity ratio [18]. As a consequence, the pump wave spatial frequency reads

$$\beta_p = \frac{\omega_p \sqrt{\epsilon_r\mu_r}}{c\gamma}. \quad (2)$$

The intrinsic impedance of a space-time permittivity- and permeability-modulated medium reads

$$\eta(z,t) = \sqrt{\frac{\mu(z,t)}{\epsilon(z,t)}} = \sqrt{\frac{\mu_0\mu_r[1 + \delta_\mu \cos(\beta_p z - \omega_p t)]}{\epsilon_0\epsilon_r[1 + \delta_\epsilon \cos(\beta_p z - \omega_p t)]}}, \quad (3)$$

which represents a space- and time-dependent intrinsic impedance. For $\delta_\mu \neq \delta_\epsilon$, Eq. (3) corresponds to a non-equilibrated space-time medium with local reflections in an infinite number of space and time discretized interfaces, i.e., $R(z_0, t) = [\eta(z_0 + \Delta z, t) - \eta(z_0, t)]/[\eta(z_0 + \Delta z, t) + \eta(z_0, t)]$ and $R(z, t_0) = [\eta(z, t_0 + \Delta t) - \eta(z, t_0)]/[\eta(z, t_0 + \Delta t) + \eta(z, t_0)]$.

Here, we consider an *equilibrated* space-time-varying medium with identical space-time modulations for the electric and magnetic properties of the medium, i.e., $\delta_\mu = \delta_\epsilon$. Therefore, the intrinsic impedance of an equilibrated space-time medium in Eq. (3) with permittivity and permeability functions in Eq. (1) reduces to

$$\eta(z,t)|_{\delta_\epsilon=\delta_\mu} = \eta_{\text{eq}} = \eta_0\eta_r, \quad (4)$$

which represents a space-time-independent intrinsic impedance yielding zero local reflections in space and time. Such an equilibrated space-time-modulated medium may be represented by a space-time-varying refractive index as

$$n(z,t)|_{\delta_\epsilon=\delta_\mu} = n_{\text{eq}} = n_r[1 + \delta_{\epsilon,\mu} \cos(\beta_p z - \omega_p t)], \quad (5)$$

where $n_r = \sqrt{\epsilon_r\mu_r}$.

To best investigate the effect of equilibration on the nonreciprocity of the space-time-modulated slab, we first derive the sonic regime interval for a general periodic space-time permittivity- and permeability-modulated medium. In the sonic and quasisonic regimes, where $\gamma \rightarrow 1$, the forward space-time modes strongly couple to each other as they acquire close phase velocities and are, hence, phase matched. In the middle of the sonic regime interval, where $v_p = v_b$ and $\gamma = 1$, all the forward space-time modes unite into a single mode and yield a shock wave by analogy with the sound-barrier breaking in acoustics [18,22]. However, in the sonic and quasisonic regimes, the backward space-time modes separate from each other. Therefore, the space-time-modulated medium exhibits its maximal nonreciprocity in the quasisonic and sonic regimes. It may be shown that the sonic regime interval is proportional to the nonreciprocity of the space-time-modulated medium, where in a reciprocal space-time-modulated medium with vanishingly small pumping strength, the sonic regime interval tends to zero.

To derive the sonic regime interval of a space-time permittivity- and permeability-modulated medium, we may follow a similar procedure as in Ref. [18] yielding

$$\gamma_{s,l} = \frac{1}{\sqrt{(1 + \delta_\epsilon)(1 + \delta_\mu)}} \leq \gamma \leq \frac{1}{\sqrt{(1 - \delta_\epsilon)(1 - \delta_\mu)}} = \gamma_{s,u}, \quad (6)$$

with $\gamma_{s,l}$ and $\gamma_{s,u}$ being the lower and upper boundaries of the sonic regime interval. Hence, the sonic regime of an equilibrated space-time-modulated medium, i.e., $\delta_\mu = \delta_\epsilon$, reads

$$\frac{1}{(1 + \delta_{\epsilon,\mu})} \leq \gamma_{s,\text{eq}} \leq \frac{1}{(1 - \delta_{\epsilon,\mu})}. \quad (7)$$

It may be seen from Eq. (7) that the sonic regime interval of an equilibrated space-time-varying medium is more than twice the nonequilibrated space-time permittivity-modulated medium with $\delta_\mu = 0$ [18]. Such an enhanced sonic regime interval represents a highly enhanced quasisonic nonreciprocity, which we demonstrate later.

III. ANALYSIS OF SPACE-TIME PERMITTIVITY- AND PERMEABILITY-MODULATED MEDIA

A. General field solution and dispersion relation

The electric and magnetic properties of the slab assume periodic modulation in both space and time, with spatial and temporal frequencies β_p and ω_p . Therefore, considering TM_x , E_x , and H_y polarization, the electric and magnetic fields inside the slab may be expressed in the form superposition of double-space-time Bloch-Floquet harmonics as

$$\mathbf{E}_S(z, t) = \hat{\mathbf{x}} e^{-i(\beta_0 z - \omega_0 t)} \sum_{n=-\infty}^{\infty} E_n e^{-in(\beta_p z - \omega_p t)}, \quad (8a)$$

$$\mathbf{H}_S(z, t) = \hat{\mathbf{y}} e^{-i(\beta_0 z - \omega_0 t)} \sum_{n=-\infty}^{\infty} H_n e^{-in(\beta_p z - \omega_p t)}, \quad (8b)$$

where β_0 and ω_0 represent, respectively, the spatial and temporal frequencies of the fundamental temporal and spatial harmonics, i.e., $n = 0$. Since the slab assumes no variation in the x and y directions, $\partial \mathbf{E}_S / \partial x = 0$, $\partial \mathbf{E}_S / \partial y = 0$. Hence, $\nabla \times \mathbf{E}_S = \hat{\mathbf{y}} \partial E_x(z, t) / \partial z$ and $\nabla \times \mathbf{H}_S = -\hat{\mathbf{x}} \partial H_y(z, t) / \partial z$. As a result, the sourceless Maxwell equations read

$$\frac{\partial E_x(z, t)}{\partial z} = -\frac{\partial [\mu(z, t) H_y(z, t)]}{\partial t}, \quad (9a)$$

$$\frac{\partial H_y(z, t)}{\partial z} = -\frac{\partial [\epsilon(z, t) E_x(z, t)]}{\partial t}. \quad (9b)$$

We next inject Eqs. (1b), (8a), and (8b) into Eq. (9a) and take the spatial and temporal derivatives. Afterwards, the result will be truncated to $2N + 1$ terms, and may be cast in the matrix form as

$$\mathbf{E} = \mathbf{Z}(\omega) \mathbf{H}, \quad (10a)$$

$$\mathbf{H} = \mathbf{Y}(\omega) \mathbf{E}, \quad (10b)$$

where $\mathbf{E} = [E_{-N} \cdots E_0 \cdots E_N]^T$, $\mathbf{H} = [H_{-N} \cdots H_0 \cdots H_N]$, and

$$\mathbf{Z}(\omega) = \eta_0 \eta_r \gamma \begin{bmatrix} v_{-N} & \frac{\delta_\mu}{2} v_{-N} & 0 & \cdots & 0 \\ \frac{\delta_\mu}{2} v_{-N+1} & v_{-N+1} & \frac{\delta_\mu}{2} v_{-N+1} & \cdots & 0 \\ 0 & \frac{\delta_\mu}{2} v_{-N+2} & v_{-N+2} & \cdots & 0 \\ \vdots & \vdots & \vdots & \ddots & \vdots \\ 0 & 0 & 0 & \cdots & v_N \end{bmatrix}, \quad (10c)$$

$$\mathbf{Y}(\omega) = \frac{\gamma}{\eta_0 \eta_r} \begin{bmatrix} v_{-N} & \frac{\delta_\epsilon}{2} v_{-N} & 0 & \cdots & 0 \\ \frac{\delta_\epsilon}{2} v_{-N+1} & v_{-N+1} & \frac{\delta_\epsilon}{2} v_{-N+1} & \cdots & 0 \\ 0 & \frac{\delta_\epsilon}{2} v_{-N+2} & v_{-N+2} & \cdots & 0 \\ \vdots & \vdots & \vdots & \ddots & \vdots \\ 0 & 0 & 0 & \cdots & v_N \end{bmatrix}, \quad (10d)$$

where $v_n = (\omega_0 / \omega_p + n) / (\beta_0 / \beta_p + n)$. Injecting Eq. (10b) into Eq. (10a) yields

$$\mathbf{K}(\omega) \mathbf{E} = 0, \quad (11a)$$

where

$$\mathbf{K}(\omega) = [\mathbf{Z}(\omega) \mathbf{Y}(\omega) - \mathbf{I}], \quad (11b)$$

with \mathbf{I} being a $(2N + 1) \times (2N + 1)$ identity matrix. The eigenvalue problem in Eq. (11a) has nontrivial solutions if

$$\det[\mathbf{K}(\omega)] = 0. \quad (12)$$

Equation (12) represents the dispersion relation, which is further studied in Sec. IV

B. Application of boundary conditions

The forward problem assumes a TM_{yz} or E_x incident electric field $\mathbf{E}_I^F(z, t) = \hat{\mathbf{x}} E_0 \exp[-i(k_0 z - \omega_0 t)]$, where E_0 represents the amplitude of the incident field and $k_0 = \omega_0 / v_r$. The corresponding incident magnetic field reads $\mathbf{H}_I^F(z, t) = \hat{\mathbf{y}} E_0 / \eta_1 \exp[-i(k_0 z - \omega_0 t)]$, with $\eta_1 = \sqrt{\mu_0 \mu_r / (\epsilon_0 \epsilon_r)}$ the intrinsic impedance of region 1. The reflected electric field consists of an infinite number of reflected space-time harmonics propagating in the $-z$ direction, as $\mathbf{E}_R^F(z, t) = \hat{\mathbf{x}} \sum_n E_{rn}^F \exp[i(k_{0n} z + \omega_n t)]$, and the corresponding magnetic fields read $\mathbf{H}_R^F(z, t) = -\hat{\mathbf{y}} \sum_n E_{rn}^F / \eta_1 \exp[i(k_{0n} z + \omega_n t)]$, where $k_{0n} = (\omega_0 + n\omega_p) / v_r$. The transmitted electric and magnetic fields outside the slab may be expressed as $\mathbf{E}_T^F(z, t) = \hat{\mathbf{x}} \sum_n E_{tn}^F \exp[-i(k_{0n} z - \omega_n t)]$ and $\mathbf{H}_T^F(z, t) = \hat{\mathbf{y}} \sum_n E_{tn}^F / \eta_3 \exp[-i(k_{0n} z - \omega_n t)]$, where $\eta_3 = \eta_1$.

To find the unknown coefficients of the electric and magnetic fields inside the slab, i.e., E_{np} and H_{np} in Eq. (8) and the unknown coefficients of the electric and magnetic fields outside the slab E_{rn}^F , H_{rn}^F , E_{tn}^F , and H_{tn}^F , we enforce the continuity of the tangential components of the electromagnetic fields at $z = 0$ and $z = L$. Considering the electric and magnetic fields inside the slab given in Eqs. (8a) and (8b), the electric field continuity condition between regions 1 and 2 at $z = 0$, $E_{1x}(0, t) = E_{2x}(0, t)$ reduces to

$$\delta_{n0}E_0 + E_{tn}^F = \sum_{p=-\infty}^{\infty} E_{np}^F, \quad (13a)$$

while the electric field continuity condition between regions 2 and 3 at $z = L$, $E_{2x}(L, t) = E_{3x}(L, t)$ reads

$$\sum_{p=-\infty}^{\infty} E_{np}^F e^{-j\beta_{np}L} = E_{tn}^F e^{-jk_{0n}L}. \quad (13b)$$

Similarly, the magnetic field continuity condition between regions 1 and 2 at $z = 0$, $H_{1y}(0, t) = H_{2y}(0, t)$ reduces to

$$\sqrt{\frac{\epsilon_0\epsilon_r}{\mu_0\mu_r}}\delta_{n0}E_0 - \sqrt{\frac{\epsilon_0\epsilon_r}{\mu_0\mu_r}}E_{tn}^F = \sum_{p=-\infty}^{\infty} H_{np}^F, \quad (14a)$$

and the magnetic field continuity condition between regions 2 and 3 at $z = L$, $H_{2y}(L, t) = H_{3y}(L, t)$ simplifies to

$$\sum_{p=-\infty}^{\infty} H_{np}^F e^{-j\beta_{np}L} = \sqrt{\frac{\epsilon_0\epsilon_r}{\mu_0\mu_r}}E_{tn}^F e^{-jk_{0n}L}. \quad (14b)$$

Following the same procedure, the electric and magnetic continuity conditions at $z = 0$ and $z = L$ may be achieved for the backward problem.

C. Numerical simulation

Figure 2 plots the implemented finite-difference time-domain scheme for the numerical simulation of space-time permittivity- and permeability-modulated media. The medium is discretized to $K + 1$ spatial samples and $M + 1$ temporal samples with the steps of Δz and Δt , respectively.

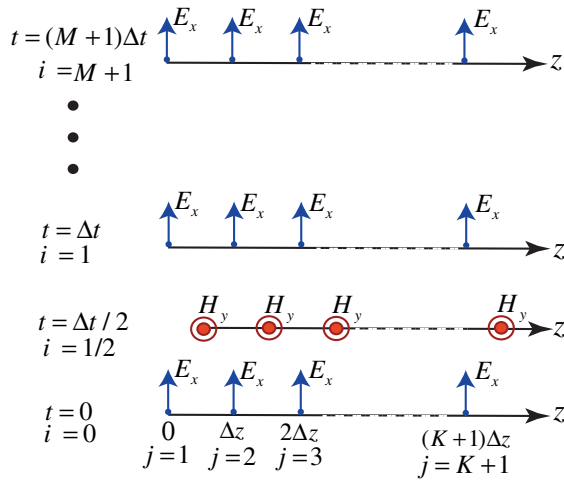


FIG. 2. General representation of the finite-difference time-domain scheme for numerical simulation of space-time permittivity- and permeability-modulated media.

We first expand the Maxwell equations in Eqs. (9a) and (9b). Then, the finite-difference discretized forms for the electric and magnetic fields may be simplified to

$$H_y|_{j+1/2}^{i+1/2} = \left(1 - \Delta t \frac{\mu'|_{j+1/2}^{i-1/2}}{\mu|_{j+1/2}^i}\right) H_y|_{j+1/2}^{i-1/2} - \frac{\Delta t/\Delta z}{\mu|_{j+1/2}^i} (E_x|_{j+1}^i - E_x|_j^i), \quad (15a)$$

$$E_x|_j^{i+1} = \left(1 - \frac{\Delta t \epsilon'|_j^i}{\epsilon|_j^{i+1/2}}\right) E_x|_j^i - \frac{\Delta t/\Delta z}{\epsilon|_j^{i+1/2}} (H_y|_{j+1/2}^{i+1/2} - H_y|_{j-1/2}^{i+1/2}), \quad (15b)$$

where $\mu' = \partial\mu(z, t)/\partial t = -\omega_p\mu_0\mu_r\delta_\mu \sin(\beta_p z - \omega_p t)$ and $\epsilon' = \partial\epsilon(z, t)/\partial t = -\omega_p\epsilon_0\epsilon_r\delta_\epsilon \sin(\beta_p z - \omega_p t)$.

IV. DISPERSION DIAGRAMS

This section studies the effect of equilibrium in the electric and magnetic properties of spatiotemporally modulated media. This may be best accomplished by analysis of the dispersion diagrams of general space-time permittivity- and permeability-modulated media. Following Ref. [18], it may be shown that the analytical solution based on the Bloch-Floquet decomposition of electromagnetic fields in Sec. III converges everywhere except inside the sonic regime interval in Eq. (6). Moreover, the accuracy of the analytical results, i.e., for the dispersion relation in Eq. (12), the electric field in Eq. (11a), and the magnetic field in Eq. (10b), depends on the truncation error and is proportional to the number of considered space-time harmonics N in the analysis, where $N \rightarrow \infty$ provides an accurate solution for all harmonics. However, as it is always desired to truncate the series in Eqs. (8a) and (8b) at the lowest possible term, we must then ensure the accuracy of the solution for the desired harmonics through the periodicity of the dispersion diagram. Since the slab is periodically modulated in space and time, its accurate dispersion diagram will be constituted of an infinite set of *periodic* forward straight lines with distances $\Delta\beta^+$ and an infinite set of *periodic* backward straight lines with distances $\Delta\beta^-$ [18]. For a given N , the dispersion diagram of the desired harmonics should be periodic, otherwise, one must increase the N to achieve a more accurate result. Here, we consider $N = 90$ to achieve an accurate solution for at least the first 20 harmonics, i.e., for $|n| < 20$.

The $\mathbf{K}(\omega)$ in the dispersion relation in Eq. (12) is constituted of $(2N + 1) \times (2N + 1)$ elements, where

$$K_{n,n} = v_n - \frac{1}{v_n \gamma^2} + \frac{\delta_\epsilon \delta_\mu}{4} (v_{n-1} + v_{n+1}), \quad (16a)$$

$$K_{n,n\pm 1} = \frac{\delta_\epsilon}{2} v_n + \frac{\delta_\mu}{2} v_{n\pm 1}, \quad (16b)$$

$$K_{n,n\pm 2} = \frac{\delta_\epsilon \delta_\mu}{4} v_{n\pm 1}, \quad (16c)$$

considering $K_{1,1} = v_n + \delta_\epsilon \delta_\mu v_{n+1}/4 - 1/(v_n \gamma^2)$ and $K_{2N+1,2N+1} = v_n + \delta_\epsilon \delta_\mu v_{n-1}/4 - 1/(v_n \gamma^2)$. In Eq. (16), $v_{n-1} = (\omega_0/\omega_p + n - 1)/(\beta_0/\beta_p + n - 1)$ and $v_{n+1} = (\omega_0/\omega_p + n + 1)/(\beta_0/\beta_p + n + 1)$. It may be seen from Eq. (16) that in a space-time permittivity-modulated medium, i.e., $\delta_\mu = 0$ [18,23], the strength of the synchronization and photonic transitions occurs from the mode n to its two adjacent modes (lower and upper modes, i.e., $n - 1$ and $n + 1$) and is governed by the term $\delta_\epsilon/2$. As a consequence, increasing the pumping strength δ_ϵ yields stronger transition between the adjacent space-time modes. By contrast, as Eq. (16) reveals, in a space-time permittivity- and permeability-modulated medium to any excited mode n , it makes photonic transitions to its four adjacent modes (two lower and two upper modes, i.e., $n - 1$, $n + 1$, $n - 2$, and $n + 2$), leading to much stronger energy transitions between an infinite number of propagating modes. Moreover, it may be seen from Eq. (16) that for a nonzero permeability pumping strength $\delta_\mu > 0$, the medium provides enhanced coupling and energy transition between the space-time modes. Furthermore, considering an equilibrium in electric and magnetic properties of the medium, i.e., $\delta_\mu = \delta_\epsilon$ in Eq. (16b), photonic band gaps disappear in the medium.

We first investigate the effect of equilibration on the photonic band gaps in conventional nonequibrated space-time-modulated media. Figure 3 plots the normal incidence dispersion diagram of a subsonic space-time-modulated medium ($\gamma = 0.15$) computed using Eq. (12) with the electric permittivity in Eq. (1a) and magnetic permeability in Eq. (1b). This diagram is formed by the infinite periodic set of $\beta_0/\beta_p - \omega_0/\omega_p$ straight lines labeled by n, p . For a given frequency, ω_0 corresponds an infinite number of modes labeled by p , themselves composed of an infinite number of forward and backward space-time harmonics labeled by n , i.e., $\beta_{0p}^\pm + n\beta_p, \omega_0 + n\omega_p$. Each curve represents a mode excited at a given frequency ω_0 , where it also represents the oblique space-time harmonic of another mode excited at another frequency. For a homogeneous nonperiodic (unmodulated) medium, $\delta_\epsilon = \delta_\mu = 0$, $n = 0$ is the only remaining curve, and for a vanishingly small pumping strength $\delta_\epsilon = \delta_\mu \rightarrow 0$, the medium is quasihomogeneous, where most of the energy remains in $p = 0$ forward and backward space-time modes.

Figure 3 compares the dispersion diagram of a non-equilibrated space-time permittivity-modulated medium, i.e., $\delta_\epsilon = 0.5$ and $\delta_\mu = 0$, with the one of the equilibrated space-time permittivity- and permeability-modulated

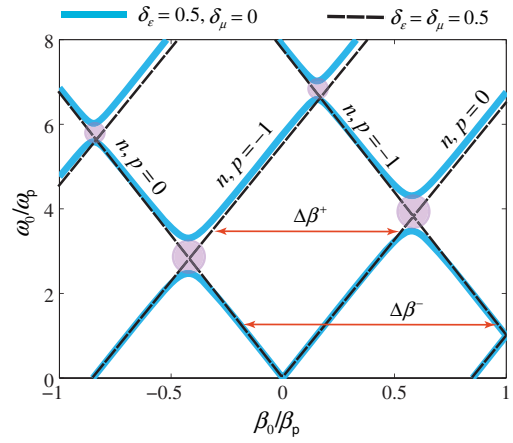


FIG. 3. Effect of equilibrium in electric and magnetic properties of spatiotemporally modulated media, i.e., $\delta_\epsilon = \delta_\mu = 0.5$, on the photonic band gaps introduced by conventional nonequibrated space-time permittivity-modulated media ($\delta_\epsilon = 0.5$ and $\delta_\mu = 0$) in the *subsonic* regime, i.e., $\gamma = 0.15$. The results are computed using Eq. (12) considering the electric permittivity in Eq. (1a) and magnetic permeability in Eq. (1b). Photonic band gaps of nonequibrated medium are highlighted with magenta circles. It should be noted that the nonreciprocity of space-time-modulated media is proportional to $\Delta\beta^- > \Delta\beta^+$, which is weak in the subsonic regime.

medium, i.e., $\delta_\epsilon = \delta_\mu = 0.5$. It may be seen in Fig. 3 that for a nonzero velocity ratio (here, $\gamma = 0.15$), the forward and backward space-time harmonics acquire different distances, i.e., $\Delta\beta^\pm = \beta_{n+1}^\pm - \beta_n^\pm$. Particularly, as γ increases, $\Delta\beta^-$ increases and $\Delta\beta^+$ decreases. For a static medium, $v_p = 0$ and both the forward and backward waves see the static period p_{stat} , and we have $\Delta\beta^\pm = \Delta\beta = 2\pi/p_{\text{stat}}$. However, as v_p increases, the forward and backward harmonics acquire different velocities relative to the modulating wave, i.e., $v^+ = v_r - v_p$ and $v^- = v_r + v_p$, respectively. This asymmetry between the velocities of the forward and backward harmonics represents two limits, $v^+ = 0$ for $v_p = v_r$ and $v^- = 2v_r$ for $v_p = v_r$, and the corresponding relative periods read $p_{\text{mov}}^+ = \infty$ for $v_p = v_r$ and $p_{\text{mov}}^- = p_{\text{stat}}/2$ for $v_p = v_r$, i.e., $p_{\text{mov}}^\pm = p_{\text{stat}} v_r / (v_r \mp v_p)$. As a result, at the limit of $\gamma = 1$, the forward harmonics acquire distances $\Delta\beta_{\text{mov}}^+/\beta_p = 0$, and the backward harmonics acquire distances $\Delta\beta_{\text{mov}}^-/\beta_p = 2$ [18]. In a conventional, nonequibrated, space-time-modulated medium, photonic band gaps occur at the space-time synchronization points, i.e., at the intersections of the forward and backward space-time modes which lie on oblique lines. These photonic band gaps of the nonequibrated medium are highlighted with magenta circles in Fig. 3. This band gap corresponds to evanescent modes, where the incident wave experiences high attenuation (reflection) as it propagates through the

medium. However, as we turn on the magnetic permeability modulation with the same pumping strength ($\delta_\mu = \delta_\epsilon = 0.5$), as a result of the equilibrium in the electric and magnetic properties of the medium, the photonic band gaps disappear. This means, no matter what the frequency of the incident wave is, it is allowed to pass through the equilibrated medium unconditionally.

The effect of the equilibration on the closing of the photonic band gaps has been highlighted in the dispersion diagram of the subsonic space-time-varying medium in Fig. 3. However, its effect on the nonreciprocity is not apparent in the subsonic regime, as the equilibrated and nonequilibrated media exhibit the same distance between the forward harmonics $\Delta\beta^+$ and backward harmonics $\Delta\beta^-$. Here, we aim to demonstrate the effect of equilibration on the nonreciprocity enhancement of unidirectionally space-time-modulated media. Figure 4(a) compares the results of the normal incidence dispersion diagram of nonequilibrated ($\delta_\epsilon = 0.5$ and $\delta_\mu = 0$) and equilibrated ($\delta_\epsilon = \delta_\mu = 0.5$) space-time-modulated media in Fig. 3 except for the quasisonic regime, i.e., $\gamma = 0.65$. This figure explicitly shows that increasing γ leads to a significant enhancement in the nonreciprocity of both cases so that the forward modes have become closer to each other ($\Delta\beta^+ \rightarrow 0$), whereas the backward harmonics have separated from each other ($\Delta\beta^- \rightarrow 2$). However, in this regime, the equilibrated medium introduces much stronger nonreciprocity $\Delta\beta^-/\Delta\beta^+$ as the distance between the forward modes $\Delta\beta^+$ of this medium is less than twice the one of the nonequilibrated medium.

Figure 4(b) highlights the fundamental forward and backward harmonics ($n = 0$) in Fig. 4(a), revealing the *tilt* of the forward wave dispersion curves in space-time permittivity- and permeability-modulated medium for $\gamma \rightarrow 1$, $\delta_\epsilon > 0$, and $\delta_\mu > 0$ (here, $\delta_\epsilon = \delta_\mu = 0.5$). In contrast to the conventional space-time permittivity-modulated medium, where forward and backward harmonics propagate with the same phase and group velocities, a space-time permittivity- and permeability-modulated medium exhibits lower phase and group velocities, i.e., $v_{\text{PH}} = \omega/\beta$ and $v_{\text{GR}} = \partial\omega/\partial\beta$, respectively, for forward harmonics. This is due to the fact that for a given frequency, the momentum of the space-time modulation (here, the space-time modulation is traveling toward the $+z$ forward direction) is injected into the medium and couples to forward harmonic waves, whereas no coupling of the space-time modulation momentum occurs to the backward (opposite) harmonic waves, and, hence, the backward dispersion curves are unaltered. Apparently, for a backward $-z$ -propagating space-time modulation, the backward dispersion curves are tilted while the forward dispersion curves are unaltered.

The pumping strength is one of the important parameters of space-time-modulated media which may significantly affect the dispersion diagram. Figures 5(a) and 5(b) plot the dispersion diagrams of the nonequilibrated space-time permittivity-modulated medium ($\delta_\mu = 0$) and equilibrated

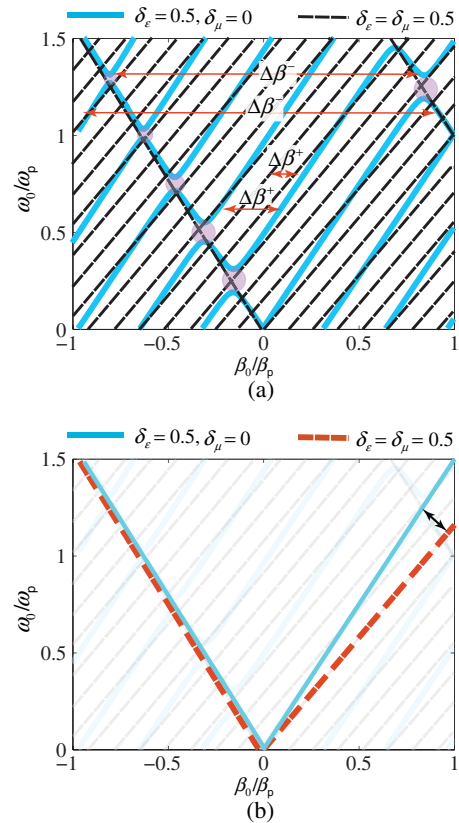


FIG. 4. Effect of equilibrium in the electric and magnetic properties of space-time media on the nonreciprocity ($\Delta\beta^-/\Delta\beta^+$) and the forward phase and group velocities in the *quasisonic* regime, i.e., $\gamma = 0.65$, with the permittivity in Eq. (1a) and permeability in Eq. (1b) computed using Eq. (12). (a) Comparison of periodic dispersion diagrams of conventional non-equilibrated periodic space-time-modulated medium, i.e., $\delta_\epsilon = 0.5$ and $\delta_\mu = 0$ corresponding to $\gamma_{s,l} = 0.816$, with equilibrated periodic space-time-modulated medium, i.e., $\delta_\epsilon = \delta_\mu = 0.5$ corresponding to $\gamma_{s,l} = 0.666$. Photonic band gaps of non-equilibrated medium are highlighted with magenta circles. (b) Tilt of the *forward* lines in the dispersion diagram of equilibrated periodic space-time-modulated medium in (b) is highlighted. Such an asymmetric tilt yields a decrease of the phase and group velocities for the forward harmonics (different velocities for forward and backward harmonics).

space-time-modulated medium ($\delta_\epsilon = \delta_\mu$) in the quasisonic regime and for two different pumping strengths, i.e., $\delta = 0.1$ and 0.5 . It may be seen from Fig. 5(a) that in a non-equilibrated space-time permittivity-modulated medium, enhancing the modulation strength from $\delta = 0.1$ to 0.5 has no significant effect on the nonreciprocity; i.e., the ratio of the distance between the forward and backward harmonics $\Delta\beta^-/\Delta\beta^+$ is almost constant for both cases. By contrast, in an equilibrated space-time-modulated medium [Fig. 5(b)], enhancing the modulation depth from $\delta = 0.1$ to 0.5 significantly increases the nonreciprocity, as the ratio of the distance between the forward and backward modes for $\delta_\mu = \delta_\epsilon = 0.5$ is almost 3 times that of the one for the

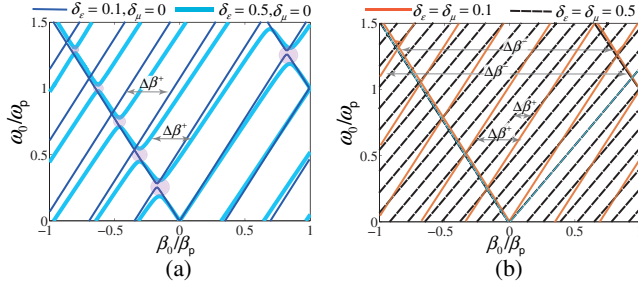


FIG. 5. Effect of pumping strength enhancement on the dispersion diagrams of periodically space-time-modulated media with the electric permittivity in Eq. (1a) and magnetic permeability in Eq. (1b) computed using Eq. (12) for $\gamma = 0.65$. (a) Non-equilibrated space-time-modulated medium ($\delta_\mu = 0$) with the modulation strengths of $\delta_\epsilon = 0.1$ and $\delta_\epsilon = 0.5$. (b) Equilibrated space-time-modulated medium with pumping strengths of $\delta_\mu = \delta_\epsilon = 0.1$ and $\delta_\mu = \delta_\epsilon = 0.5$.

same medium with $\delta_\mu = \delta_\epsilon = 0.1$, and, hence, a substantial number of forward space-time modes contribute to the fields.

Finally, Figs. 6(a) and 6(b) show the photonic band gaps of the nonequilibrated space-time permittivity-modulated medium for two different pumping strengths and velocity ratios, i.e., ($\delta_\epsilon = 0.5$, $\gamma = 0.65$) and ($\delta_\epsilon = 0.2$, $\gamma = 0.8$). Clearly, no photonic band gap exists in the equilibrated case. These figures explicitly demonstrate the design flexibility of the equilibrated space-time-modulated medium as follows. The equilibrated medium with low pumping strength of $\delta_\mu = \delta_\epsilon = 0.2$ with $\gamma = 0.8$ introduces the same amount of nonreciprocity ($\Delta\beta^+$, where $\Delta\beta^- \rightarrow 2$ is almost constant for both cases) as $\delta_\mu = \delta_\epsilon = 0.5$. This property is very important, as it practically represents saving an important amount of pumping wave energy.

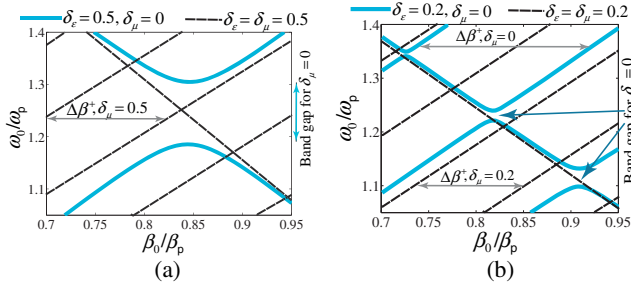


FIG. 6. Comparison of the dispersion diagrams for the quasi-sonic regime of nonequilibrated space-time-modulated medium ($\delta_\mu = 0$) and equilibrated space-time-modulated medium ($\delta_\mu = \delta_\epsilon$), with the permittivity in Eq. (1a) and permeability in Eq. (1b) computed using Eq. (12). (a) $\gamma = 0.65$ ($\gamma_{s,1} = 0.816$ for nonequilibrated medium and $\gamma_{s,1} = 0.666$ for the equilibrated medium) with $\delta_\mu = 0.5$ and $\delta_\epsilon = 0.5$. (b) $\gamma = 0.8$ ($\gamma_{s,1} = 0.913$ for nonequilibrated medium and $\gamma_{s,1} = 0.833$ for equilibrated medium) and $\delta_\mu = 0.2$ and $\delta_\epsilon = 0.2$.

V. TRANSMISSION AND REFLECTION

This section provides a comparison between the wave scattering from equilibrated space-time-modulated and the conventional space-time permittivity-modulated medium. The electromagnetic scattering from such a slab is studied using the FDTD simulations presented in Sec. III C. We first investigate the scattering from the conventional, nonequilibrated, space-time-modulated slab with $\delta_\epsilon > 0$ and $\delta_\mu = 0$. Next, we compare the results with those of an equilibrated space-time-modulated slab, where $\delta_\epsilon = \delta_\mu > 0$.

Consider a plane wave with frequency $\omega_0 = 2\pi \times 1.5$ GHz impinging on a slab with conventional sinusoidally space-time-modulated permittivity in Eq. (1), with $\delta_\epsilon = 0.02$ and $\delta_\mu = 0$. The slab assumes $\omega_p = 2\pi \times 0.2$ GHz, $L = 20\lambda_0$, and velocity ratio $\gamma = 1$. Figure 7(a) plots the FDTD numerical results for the forward problem amplitude of the scattered electric fields from this slab. In this scheme, a point source is located at $z = z_0$ and shines a plane wave toward the $+z$ direction at fundamental frequency ω_0 ($n = 0$). As the wave impinges to the slab interface at $z = 0$ and propagates through it, part of the wave passes through the slab while generating space-time harmonic waves at $n < 0$ and $n > 0$. However, due to the space-time reflections, part of the wave reflects back toward the $-z$ direction, travels toward the $-z$ -direction, passes the sources, and is absorbed at the left boundary of the simulation domain.

Figure 7(b) plots the same FDTD numerical results but for an equilibrated space-time permittivity- and permeability-modulated slab in Fig. 1, with *weak* pumping strength of $\delta_\mu = \delta_\epsilon = 0.02$. The slab parameters are the same as in Fig. 7(a) except for the nonzero permeability modulation of $\delta_\mu = 0.02$. As the incident wave propagates through the slab, it generates strong space-time harmonics. By contrast with the slab in Fig. 7(a), here none of the space-time harmonics reflect back toward the $-z$ direction due to the equilibration in the space-time modulation of the electric and magnetic properties of the medium. Negligible reflection may be seen in Fig. 7(b), which is due to the sampling error in the numerical simulation scheme, i.e., $\Delta z = \lambda_0/60 \neq 0$ and $\Delta t = \Delta z/c \neq 0$.

Figure 7(c) compares the spectra of the transmitted space-time harmonics (for the forward problem wave incidence) for the conventional and equilibrated space-time-modulated slabs with the time-domain response, respectively, in Figs. 7(a) and 7(b). It may be seen from this figure that the equilibrated slab provides the required momentum for a strong transition of the energy from the fundamental harmonic at $n = 0$ to higher-order space-time harmonics, i.e., at $n = \dots, -2, -1, +1, +2, \dots$, where the amplitude of the fundamental harmonic is significantly weakened, i.e., lower than -19 dB. In contrast, the conventional slab does not provide the required momentum for

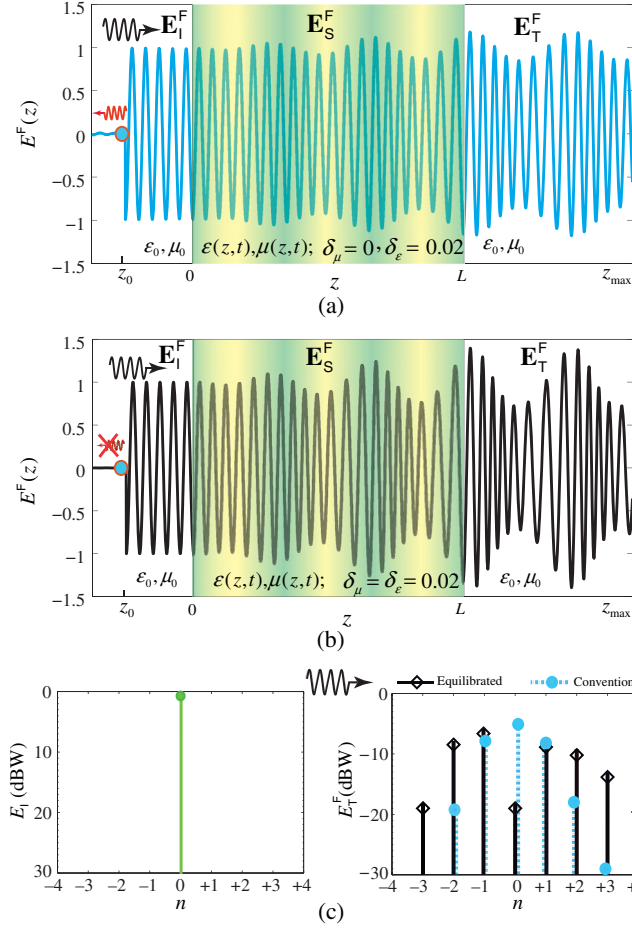


FIG. 7. FDTD numerical simulation results for the *forward* problem electromagnetic scattering from a sinusoidally space-time-modulated slab with $\delta_\epsilon = 0.02$. The parameters of the incident wave and the slab are $\omega_0 = 2\pi \times 1.5$ GHz, $\omega_p = 2\pi \times 0.2$ GHz, $L = 20\lambda_0$, and $\gamma = 1$. (a) Time-domain response for the scattering from the conventional permittivity-modulated slab ($\delta_\mu = 0$) showing the reflected wave on the right side before $z = z_0$, whereas the transmitted wave on the right side includes weak space-time harmonics. (b) Time-domain response for the scattering from equilibrated permittivity- and permeability-modulated slab ($\delta_\mu = \delta_\epsilon = 0.02$) showing the zero reflection on the left side, whereas the transmitted wave on the right side is composed of strong space-time harmonics. (c) Comparison of the forward problem harmonic generation in conventional and equilibrated space-time-modulated media. Frequency domain response for the incident wave (left side) and transmitted wave (right side). Particularly, $n = 0$ corresponds to the fundamental harmonic at $\omega_0 = 2\pi \times 1.5$ GHz, and $n = +1$ corresponds to the first higher-order harmonic at $\omega_{+1} = \omega_0 + \omega_p = 2\pi \times (1.5 + 0.2)$ GHz.

strong transition of the energy to higher-order space-time harmonics, and most of the energy is still residing in the fundamental harmonic.

We next compare the *backward* problem wave scattering from the conventional and equilibrated space-time slabs in Figs. 7(a) and 7(b), respectively. In Fig. 8(a), a plane wave

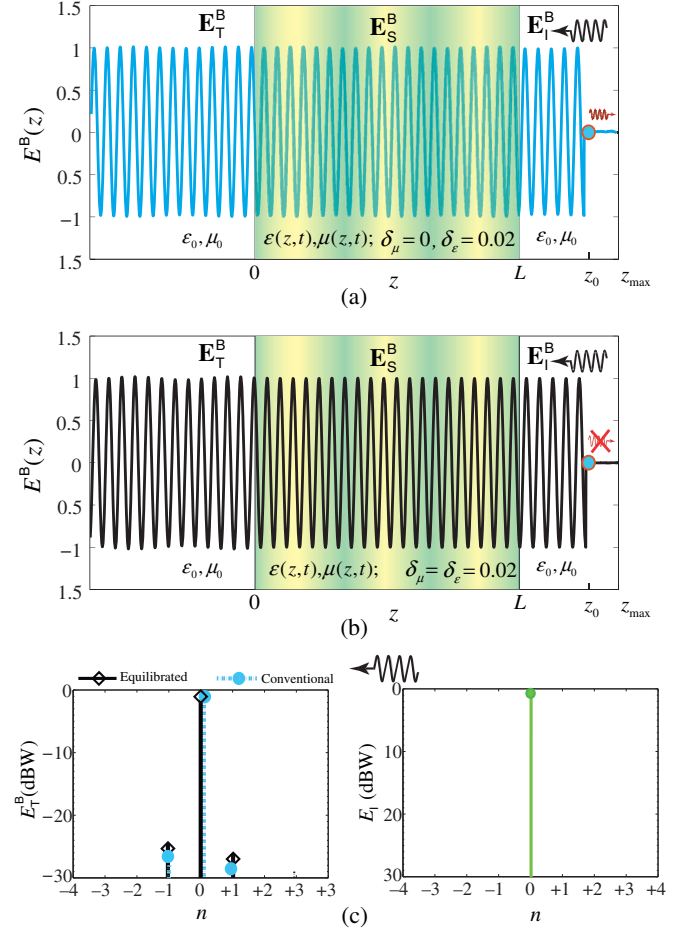


FIG. 8. FDTD numerical simulation results for the *backward* problem electromagnetic scattering from a sinusoidally space-time modulated slab as in Fig. 7. (a) Time-domain response for the scattering from the conventional permittivity-modulated slab ($\delta_\mu = 0$) showing the reflected wave on the right side before $z = z_0$, and the wave passes through the slab with nearly no alteration. (b) Time-domain response for the scattering from the equilibrated permittivity- and permeability-modulated slab ($\delta_\mu = \delta_\epsilon = 0.02$) showing zero reflection on the right side, and the wave passes through the slab with nearly no alteration. (c) Comparison of the backward problem harmonic generation in conventional and equilibrated space-time modulated media. Frequency domain response for the incident wave (right side) and transmitted wave (left side).

with frequency $\omega_0 = 2\pi \times 1.5$ GHz impinges on the conventional space-time slab [same slab as in Fig. 7(a)] with sinusoidally space-time-modulated permittivity in Eq. (1), with $\delta_\epsilon = 0.02$ and $\delta_\mu = 0$. Here, the point source is located at $z = z_0$ and shines a plane wave toward the $-z$ direction at fundamental frequency ω_0 ($n = 0$). As the wave impinges to the slab interface at $z = L$, it propagates through the slab and reaches to the left side while generating quite weak and negligible space-time harmonic waves at $n < 0$ and $n > 0$. However, due to the space and time local reflections, part of the wave reflects back toward the $+z$ direction and

reaches to the right side of the simulation domain at z_{\max} . Figure 8(b) presents the backward wave scattering from the equilibrated space-time slab [same slab as in Fig. 7(b)] with sinusoidally space-time-modulated permittivity and permeability in Eq. (1), i.e., $\delta_\mu = \delta_\epsilon = 0.02$. Here, similar to the backward incidence to the conventional slab in Fig. 8(a), the wave impinges to the slab interface at $z = L$ and propagates and passes through the slab while generating very weak and negligible space-time harmonic waves at $n < 0$ and $n > 0$. However, no space and time reflections are seen on the right side of the figure.

Figure 8(c) plots the comparison of the backward problem frequency domain spectra of the transmitted space-time harmonics from the conventional and equilibrated space-time-modulated slabs, with the time-domain response, respectively, in Figs. 8(a) and 8(b). This figure shows that both the equilibrated and conventional space-time slabs provide nearly the same response for the backward problem, where the fundamental harmonic at $n = 0$ is transmitted through these slabs with quite negligible transition to higher-order harmonics with most of the energy residing with the fundamental harmonic at $n = 0$ ($\omega_0 = 2\pi \times 1.5$ GHz). Comparison of the wave transmissions for forward and backward problems, respectively, in Figs. 7 and 8, reveals the highly enhanced nonreciprocity of the equilibrated space-time slab, as well as its zero space and time reflections. Such reflection-free and strong nonreciprocal frequency generation is expected to pave the way for developing a class of integrated nonreciprocal devices as in Refs. [17,30,31].

Figures 9(a) and 9(b) compare the isolation between the forward and backward transmissions for each harmonic through the conventional [Figs. 7(a) and 8(a)] and equilibrated [Figs. 7(b) and 8(b)] space-time slabs. It may be seen from Fig. 9 that equilibrium in the electric and magnetic

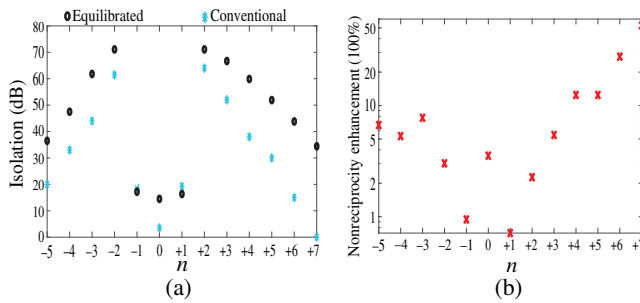


FIG. 9. Comparison of the nonreciprocity in conventional and equilibrated space-time-modulated slabs in Figs. 7 and 8. (a) Isolation between forward and backward transmissions for each harmonic, where $n = 0$ represents the fundamental harmonic at $\omega_0 = 2\pi \times 1.5$ GHz, $n = +1$ corresponds to the first higher-order harmonic at $\omega_{+1} = \omega_0 + \omega_p = 2\pi \times (1.5 + 0.2)$ GHz, etc. (b) Nonreciprocity-enhanced equilibrated space-time slab in comparison with the nonreciprocity provided by the conventional space-time slab. This result is achieved by comparing the results in (a), where the vertical axis is in logarithmic scale.

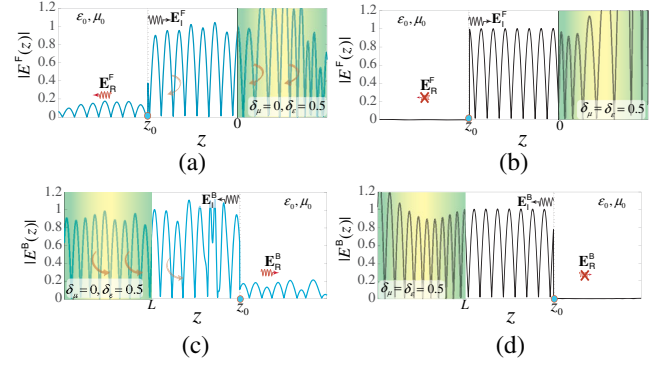


FIG. 10. Electromagnetic wave incidence and reflection from the same space-time-modulated slab in Figs. 7–9 only with stronger modulation strength of $\delta = 0.5$. We consider such a strong modulation strength only to highlight the space and time reflections in conventional space-time media. (a) Forward incidence to the conventional space-time slab with $\delta_\mu = 0$ and $\delta_\epsilon = 0.5$. (b) Forward incidence to the equilibrated space-time slab with $\delta_\mu = \delta_\epsilon = 0.5$. (c) Backward incidence to the conventional space-time slab with $\delta_\mu = 0$ and $\delta_\epsilon = 0.5$. (d) Backward incidence to the equilibrated space-time slab with $\delta_\mu = \delta_\epsilon = 0.5$.

properties of the space-time-modulated slab has significantly enhanced the nonreciprocity of the harmonics. Particularly, the nonreciprocity of the fundamental harmonic (which is the most important harmonic and desired to be highly isolated [18,28,31]) is more than 360% enhanced, where the nonreciprocity of most of the harmonics is more than 220% enhanced. Nonreciprocal subharmonic generation represents one of the most interesting applications of space-time-modulated media to be further studied [28], where the nonreciprocity of higher-order harmonics, e.g., $n = +6$ and $n = +7$, is highly coveted.

To highlight the space and time reflections in conventional space-time slabs and to best investigate the reflection from equilibrated space-time slabs, we next increase the pumping strength to $\delta = 0.5$. Figures 10(a) and 10(b) plot the *forward* problem wave reflection, respectively, from conventional and equilibrated slabs. It is obvious that the conventional slab exhibits strong space and time local reflections shown by E_R , whereas the equilibrated slab presents no space and time local reflections. Figures 10(c) and 10(d) plot the *backward* problem wave reflection, respectively, from the same conventional and equilibrated slabs. It may be seen from this figure that backward excitation of the conventional space-time slab yields space and time reflections nearly similar and equal to those of the forward problem.

VI. SPECULATION ON PRACTICAL IMPLEMENTATION SCENARIOS

Practical implementation of the space-time permittivity- and permeability-modulated slab in Fig. 1 represents an interesting topic of research. Spatiotemporal modulation of

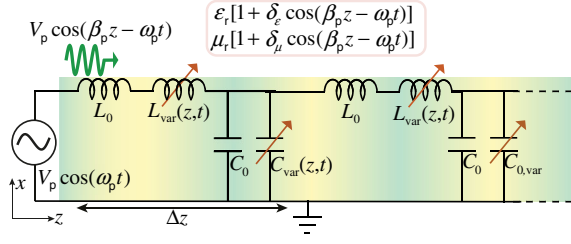


FIG. 11. Circuit model for a sinusoidally space-time permittivity- and permeability-modulated transmission line in Fig. 1. In this scheme, the pump wave spatiotemporally modulates both the permittivity (variable capacitors) and permeability (variable inductors) of the structure.

the permeability is experimentally demonstrated in Ref. [21], and the one for permittivity is experimentally demonstrated in Refs. [18,28,31,34,40,41]. Recently, in Ref. [28], a slab with spatiotemporally varying permittivity and spatially varying permeability was experimentally implemented, yielding a quasiperfect frequency mixing.

Here, we provide some speculations about practical implementation scenarios of spatiotemporally varying permittivity- and permeability-modulated slabs. Even though such a spatiotemporally varying medium may seem hard to realize, the author believes that there exist quite a few ways to accomplish it, especially with the advent of metamaterials and the fact that as shown in Sec. V, such a slab is capable of providing giant nonreciprocity for a weak modulation, e.g., $\delta_\mu = \delta_\epsilon = 0.02$.

Figure 11 sketches a circuit model for the realization of the sinusoidally space-time permittivity- and permeability-modulated slab in Fig. 1. This circuit is formed by an array of subwavelength-spaced unit cells, each of which is composed of a variable inductor and a variable capacitor, respectively, in series and parallel with the intrinsic inductance and capacitance of the transmission line. A sinusoidal harmonic wave, i.e., $V_P \cos(\omega_P t)$ is pumped into the system and propagates toward the $+z$ direction, yielding $V_P \cos(\beta_P z - \omega_P t)$ and spatiotemporally modulates the variable inductors and variable capacitances. As a consequence, such a structure with highly enhanced nonreciprocity shown in Sec. V requires the same pumped energy as a conventional space-time permittivity-modulated structure [18,40,41]. The realization of a microwave and optical version of this circuit may be accomplished by using varactors or p - n junctions [18,40] (as variable capacitances), and varactor- and thyristor-based variable inductors [42–48].

Another interesting scheme for the realization of a permeability- and permittivity-modulated slab consists of an array of cascaded omega metamaterials [49] loaded with varactors. Omega metamaterials interact with both electric and magnetic components of light and represent a class of metamaterials with tailored permittivity and permeability.

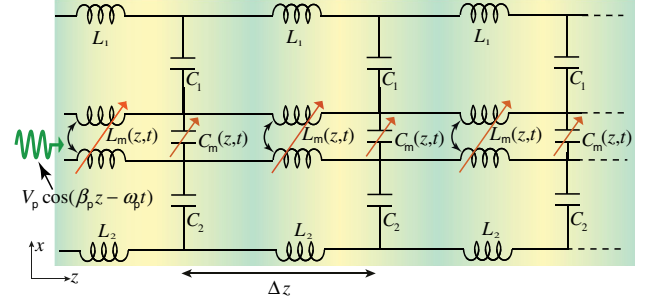


FIG. 12. Circuit model for a sinusoidally space-time permittivity- and permeability-modulated coupled transmission line. In this scheme, the pump wave spatiotemporally modulates the mutual permittivity and the mutual permeability of the coupled transmission line represented by variable mutual capacitors and variable mutual inductors, respectively.

Figure 12 shows another potential approach for the realization of a space-time permittivity- and permeability-modulated structure. This circuit model is composed of a coupled transmission line with space-time-modulated mutual inductance and mutual capacitance, i.e., $L_m(z, t)$ and $C_m(z, t)$, respectively. Such a structure may be realized following the technique reported in Ref. [21] or using a coupled microstrip transmission line and loaded with array of subwavelength-spaced varactors in a way to provide variable inductance and capacitances. In this scheme, one may utilize varactor-loaded omega or ring particles for achieving permeability modulation.

It should be noted that in a space-time-modulated medium, the modulation frequency is usually set at low radio frequencies, e.g., at the microwave regime or lower, even if the operation frequency is at terahertz or optical frequencies [18,40]. As a result, varactor diodes or other semiconductors may represent the best choice for the realization of the required variable permittivity and permeability.

VII. CONCLUSIONS

We investigate the effect of equilibrium in the electric and magnetic properties of periodic space-time-modulated media. We show that a space-time permittivity- and permeability-modulated medium with identical electric and magnetic modulation strengths, i.e., an equilibrated space-time-modulated medium, exhibits giant linear nonreciprocity, zero space-time reflections, and zero photonic band gap. Interestingly, such an enhanced nonreciprocity is accompanied by a larger sonic regime interval which provides extra design freedom for achieving strong nonreciprocity by a weak pumping strength. A rigorous analytical solution is derived for the investigation of wave propagation and scattering from general periodic space-time permittivity- and permeability-modulated media. Moreover, highly enhanced nonreciprocity and zero band gap in an equilibrated space-time-modulated medium are

exhibited in the dispersion diagrams. Furthermore, a numerical simulation scheme is implemented providing more insight into the wave scattering from general periodic space-time permittivity- and permeability-modulated media. This theoretical and numerical demonstration of reflection-free enhanced-nonreciprocity space-time-modulated media represents the first step in developing a class of nonreciprocal devices.

-
- [1] Ronald F. Soohoo, Microwave ferrite materials and devices, *IEEE Trans. Magn.* **4**, 118 (1968).
- [2] Stéphane Capraro, Thomas Rouiller, Martine Le Berre, Jean-Pierre Chatelon, Bernard Bayard, Daniel Barbier, and Jean Jacques Rousseau, Feasibility of an integrated self-biased coplanar isolator with barium ferrite films, *IEEE Trans. Compon. Packag. Technol.* **30**, 411 (2007).
- [3] K. Suzuki and R. Hirota, Nonreciprocal millimeter-wave devices using a solid-state plasma at room temperature, *IEEE Trans. Electron Devices* **18**, 408 (1971).
- [4] Ghassan N. Jawad, Christopher I. Duff, and Robin Sloan, A millimeter-wave gyroelectric waveguide isolator, *IEEE Trans. Microwave Theory Tech.* **65**, 1249 (2017).
- [5] S. Tanaka, N. Shimomura, and K. Ohtake, Active circulators —The realization of circulators using transistors, *Proc. IEEE* **53**, 260 (1965).
- [6] Z. Wang, Z. Wang, J. Wang, B. Zhang, J. Huangfu, J. D. Joannopoulos, M. Soljai, and L. Rana, Gyrotropic response in the absence of a bias field, *Proc. Natl. Acad. Sci. U.S.A.* **109**, 13194 (2012).
- [7] Sajjad Taravati, Bakhtiar A. Khan, Shulabh Gupta, Karim Achouri, and Christophe Caloz, Nonreciprocal nongyrotropic magnetless metasurface, *IEEE Trans. Antennas Propag.* **65**, 3589 (2017).
- [8] Marin Soljačić, Chiyun Luo, John D. Joannopoulos, and Shanhui Fan, Nonlinear photonic crystal microdevices for optical integration, *Opt. Lett.* **28**, 637 (2003).
- [9] V. K. Valev, J. J. Baumberg, B. De Clercq, N. Braz, X. Zheng, E. J. Osley, S. Vandendriessche, M. Hojeij, C. Blejean, C. G. Mertens, J. Biris, V. Volskiy, M. Ameloot, Y. Ekinci, G. A. E. Pandenbosch, P. A. Warburton, V. V. Moshchalkov, N. C. Panoiu, and T. Verbiest, Nonlinear superchiral meta-surfaces: Tuning chirality and disentangling non-reciprocity at the nanoscale, *Adv. Mater.* **26**, 4074 (2014).
- [10] Long Chang, Xiaoshun Jiang, Shiyue Hua, Chao Yang, Jianming Wen, Liang Jiang, Guanyu Li, Guanzhong Wang, and Min Xiao, Parity-time symmetry and variable optical isolation in activepassive-coupled microresonators, *Nat. Photonics* **8**, 524 (2014).
- [11] Ahmed M. Mahmoud, Arthur R. Davoyan, and Nader Engheta, All-passive nonreciprocal metastructure, *Nat. Commun.* **6**, 8359 (2015).
- [12] Zhong-Ming Gu, Jie Hu, Bin Liang, Xin-Ye Zou, and Jian-Chun Cheng, Broadband non-reciprocal transmission of sound with invariant frequency, *Sci. Rep.* **6**, 19824 (2016).
- [13] B. Lax and K. J. Button, *Microwave Ferrites and Ferromagnetics* (McGraw-Hill, New York, 1962).
- [14] Geert Carchon and Bart Nauwelaers, Power and noise limitations of active circulators, *IEEE Trans. Microwave Theory Tech.* **48**, 316 (2000).
- [15] Yu Shi, Zongfu Yu, and Shanhui Fan, Limitations of nonlinear optical isolators due to dynamic reciprocity, *Nat. Photonics* **9**, 388 (2015).
- [16] Joshua N. Winn, Shanhui Fan, John D. Joannopoulos, and Erich P. Ippen, Interband transitions in photonic crystals, *Phys. Rev. B* **59**, 1551 (1999).
- [17] Z. Yu and S. Fan, Complete optical isolation created by indirect interband photonic transitions, *Nat. Photonics* **3**, 91 (2009).
- [18] Sajjad Taravati, Nima Chamanara, and Christophe Caloz, Nonreciprocal electromagnetic scattering from a periodically space-time modulated slab and application to a quasisonic isolator, *Phys. Rev. B* **96**, 165144 (2017).
- [19] A. L. Cullen, A travelling-wave parametric amplifier, *Nature (London)* **181**, 332 (1958).
- [20] P. K. Tien, Parametric amplification and frequency mixing in propagating circuits, *J. Appl. Phys.* **29**, 1347 (1958).
- [21] P. K. Tien and H. Suhl, A traveling-wave ferromagnetic amplifier, *Proc. IRE* **46**, 700 (1958).
- [22] A. Oliner and A. Hessel, Guided waves on sinusoidally-modulated reactance surfaces, *IEEE Trans. Antennas Propag.* **7**, 201 (1959).
- [23] E. S. Cassedy and A. A. Oliner, Dispersion relations in time-space periodic media: Part I—Stable interactions, *Proc. IEEE* **51**, 1342 (1963).
- [24] E. S. Cassedy, Waves guided by a boundary with time-space periodic modulation, *Proc. IEEE* **112**, 269 (1965).
- [25] S. T. Peng, E. S. Cassedy, and B. Rama Rao, The sonic region for propagation in a parametric medium with harmonic pump modulation, *Proc. IEEE* **57**, 224 (1969).
- [26] R. S. Chu and T. Tamir, Guided-wave theory of light diffraction by acoustic microwaves, *IEEE Trans. Microwave Theory Tech.* **17**, 1002 (1969).
- [27] R. S. Chu and T. Tamir, Wave propagation and dispersion in space-time periodic media, *Proc. IEEE* **119**, 797 (1972).
- [28] Sajjad Taravati, Aperiodic space-time modulation for pure frequency mixing, *Phys. Rev. B* **97**, 115131 (2018).
- [29] G. M. Roe and M. R. Boyd, Parametric energy conversion in distributed systems, *Proc. IRE* **47**, 1213 (1959).
- [30] S. Taravati and C. Caloz, Space-time modulated nonreciprocal mixing, amplifying and scanning leaky-wave antenna system, in Proceedings of the IEEE International Symposium on Antennas and Propagation, Vancouver, Canada, 2015 (IEEE, New York, 2015).
- [31] Sajjad Taravati and Christophe Caloz, Mixer-duplexer-antenna leaky-wave system based on periodic space-time modulation, *IEEE Trans. Antennas Propag.* **65**, 442 (2017).
- [32] M. S. Kang, A. Butsch, and P. St. J. Russell, Reconfigurable light-driven opto-acoustic isolators in photonic crystal fibre, *Nat. Photonics* **5**, 549 (2011).
- [33] Nima Chamanara, Sajjad Taravati, Zoé-Lise Deck-Léger, and Christophe Caloz, Optical isolation based on space-time engineered asymmetric photonic bandgaps, *Phys. Rev. B* **96**, 155409 (2017).
- [34] Sajjad Taravati, Self-biased broadband magnet-free linear isolator based on one-way space-time coherency, *Phys. Rev. B* **96**, 235150 (2017).

- [35] Y. Hadad, D. L. Sounas, and A. Alù, Space-time gradient metasurfaces, *Phys. Rev. B* **92**, 100304 (2015).
- [36] A. Shaltout, A. Kildishev, and V. ShalaeV, Time-varying metasurfaces and Lorentz nonreciprocity, *Opt. Mater. Express* **5**, 2459 (2015).
- [37] Yu Shi, Seunghoon Han, and Shanhui Fan, Optical circulation and isolation based on indirect photonic transitions of guided resonance modes, *ACS Photonics* **4**, 1639 (2017).
- [38] Mohammad Mahdi Salary, Samad Jafar-Zanjani, and Hossein Mosallaei, Time-varying metamaterials based on graphene-wrapped microwires: Modeling and potential applications, *Phys. Rev. B* **97**, 115421 (2018).
- [39] Sajjad Taravati, Application of space-and time-modulated dispersion engineered metamaterials to signal processing and magnetless nonreciprocity, Ph.D. thesis, École Polytechnique de Montréal, 2017.
- [40] H. Lira, Z. Yu, S. Fan, and M. Lipson, Electrically Driven Nonreciprocity Induced by Interband Photonic Transition on a Silicon Chip, *Phys. Rev. Lett.* **109**, 033901 (2012).
- [41] Shihan Qin, Qiang Xu, and Yuanxun Ethan Wang, Nonreciprocal components with distributedly modulated capacitors, *IEEE Trans. Microwave Theory Tech.* **62**, 2260 (2014).
- [42] Volkan Turgul, Tayfun Nesimoglu, and B. S. Yarman, A study on rf/microwave tunable inductor topologies, in *Proceedings of the 13th Mediterranean Microwave Symposium (MMS), 2013* (IEEE, New York, 2013), pp. 1–4.
- [43] Jidan Al-Eryani, Herbert Knapp, Hao Li, Jonas Wursthorn, Klaus Aufinger, Soran Majied, Sabine Boguth, Rudolf Lachner, Josef Bock, and Linus Maurer, Wideband 148–188 GHz push-push VCO using variable inductance and capacitance, in *Proceedings of the 11th European Microwave Integrated Circuits Conference (EuMIC), 2016* (IEEE, New York, 2016), pp. 313–316.
- [44] Mostafa Amirpour, Saeed Akbari, Ebrahim Abbaspour Sani, and Mohammad N. Azarmanesh, Varactor based tunable inductor design, in *Proceedings of the 23rd Iranian Conference on Electrical Engineering (ICEE), 2015* (IEEE, New York, 2015), pp. 1419–1422.
- [45] Yoshiaki Yoshihara, Hirotaka Sugawara, Hiroyuki Ito, Kenichi Okada *et al.*, Wide tuning range LC-VCO using variable inductor for reconfigurable rf circuit, *IEICE Trans. Fundam. Electron. Commun. Comput. Sci.* **E88-A**, 507 (2005).
- [46] Marina Vroubel, Yan Zhuang, Behzad Rejaei, and Joachim N. Burghartz, Integrated tunable magnetic rf inductor, *IEEE Electron Device Lett.* **25**, 787 (2004).
- [47] Jason James, John Boys, and Grant Covic, A variable inductor based tuning method for ICPT pickups, in *Proceedings of the 7th International Power Engineering Conference, 2005* (IEEE, New York, 2005), pp. 1142–1146.
- [48] Matteo Tonso, J. Moren, Sjoerd W. H. de Haan, and J. A. Ferreira, Variable inductor for voltage control in distribution networks, in *Proceedings of the 2005 European Conference on Power Electronics and Applications, 2005* (IEEE, New York, 2005), pp. 1–10.
- [49] Mamdouh M. I. Saadoun and Nader Engheta, A reciprocal phase shifter using novel pseudo-chiral or ω medium, *Microwave Opt. Technol. Lett.* **5**, 184 (1992).